Single-particle, particle-pair, and multi-particle dispersion of fluid particles in forced stably stratified turbulence

Single-particle, particle-pair, and multiparticle dispersion of fluid particles in forced stably stratified turbulence

M. van Aartrijk,[1] H. J. H. Clercx,[1,a)] and K. B. Winters[2]
[1]*Fluid Dynamics Laboratory, Department of Physics, International Collaboration for Turbulence Research (ICTR) and J. M. Burgers Center for Fluid Dynamics, Eindhoven University of Technology, P.O. Box 513, 5600 MB Eindhoven, The Netherlands*
[2]*Scripps Institution of Oceanography and Department of Mechanical and Aerospace Engineering, University of California, San Diego, La Jolla, California 92093-0209, USA*

(Received 13 April 2007; accepted 21 December 2007; published online 27 February 2008)

The dispersion of fluid particles in statistically stationary stably stratified turbulence is studied by means of direct numerical simulations. Due to anisotropy of the flow, horizontal and vertical dispersion show different behavior. Single-particle dispersion in horizontal direction is similar to that in isotropic turbulence for short times, but shows a long-time growth rate proportional to $t^{2.1\pm0.1}$, larger than the classical linear diffusion limit. In vertical direction, three successive regimes can be identified: a classical t^2-regime, a plateau that scales as N^{-2}, and a diffusion limit where dispersion is proportional to t. By forcing the flow and performing long-time simulations, we are able to observe this last regime, which was predicted but not observed before in stratified turbulence. This diffusive regime is caused by molecular diffusion of the active scalar (density). The mean squared separation of particle pairs (relative dispersion) in vertical direction shows two plateaus that are not present in isotropic turbulence. They can be associated with the characteristic layered structure of the flow. In the long-time limit again a linear regime is found as for single-particle dispersion. Pair dispersion in horizontal direction behaves similar to that in isotropic turbulence except for long times. Finally, the study of multiparticle statistics in stably stratified turbulent flows is reported. The evolution of tetrads gives an impression of the shape of particle clouds. It is found that with increasing stratification, the volume of the tetrads decreases, and they become flatter and more elongated. © *2008 American Institute of Physics*. [DOI: 10.1063/1.2838593]

I. INTRODUCTION

Dispersion of particles in stratified flows plays an important role in geophysical environments. These particles can be passive or active, like aerosols in the atmospheric boundary layer and micro-organisms in coastal areas and estuaries. Including all biological and physical parameters in modeling particle dispersion is complicated, and as a starting point in this work, the effect of stratification on dispersion of passive fluid particles is considered. Homogeneous stratified turbulent flow is used here, in correspondence with previous fundamental studies. The work that has been carried out on fluid particle dispersion in homogeneous stratified turbulence is to date rather limited. Kimura and Herring[1] studied dispersion in decaying stratified turbulence by means of direct numerical simulations (DNS), and Nicolleau and Vassilicos[2] used kinematic simulations (KS) to study dispersion in nondecaying stratified turbulence. More recently, Liechtenstein *et al.*[3,4] investigated the influence of nonlinear effects on fluid particle dispersion by comparing the results of DNS simulations of decaying stratified (and rotating) turbulence with those of KS and rapid distortion theory (RDT). Some examples of experimental studies on particle dispersion in stratified turbulence can be found in Pearson *et al.*[5] As opposed to the before-mentioned numerical work, we apply forcing in our DNS of the Boussinesq equations, which makes it possible to study statistically stationary homogeneous stratified turbulence. In this way, we have been able to track particles for sufficiently long times in order to obtain long time series for calculating Lagrangian statistics.

The present study deals with turbulent flows affected by stable stratification, so the average density of the fluid is decreasing with height. Under the influence of strong stable density stratification, two sorts of motion occur simultaneously: propagating internal gravity waves and a nonpropagating nonlinear component connected with quasihorizontal motions.[6] The type of flow under consideration is homogeneous and anisotropic. In order to keep the stratified turbulence statistically stationary, energy has to be continuously added in our simulations to account for energy losses due to viscous dissipation. This has the great advantage that the relative importance of stratification effects to turbulence effects is constant in time, as opposed to decaying stratified turbulence, where the influence of stratification increases in time. There is still some discussion how these types of anisotropic flows should be forced, whether forcing should be applied to all three directions or just in the horizontal plane, and at which length scales the turbulence should be forced.[7–9] Anisotropy of the flow, and as a result also anisotropy of the dispersion, should evolve naturally from the interaction between the flow and the background density profile and should not be artificially imposed by the forcing method. To this end, different types of forcing have been

a)Electronic mail: h.j.h.clercx@tue.nl.

tested. The final choice, which best served our purposes, was forcing only at the largest scales and with equal strength in all three directions.

This study specifically aims to look at fluid particle dispersion. In view of future applications where aggregate formation might play a role, not only the spreading of single particles will be studied but also that of small clusters of particles. For homogeneous isotropic turbulence, a lot of work has been reported on both single-particle and particle-pair dispersion, experimentally but mainly using numerical simulations.[10–15] Single-particle dispersion is defined here as the mean-squared displacement of a particle from the initial position, and particle-pair dispersion is the mean-squared separation of a pair of particles. Theoretically, the spreading of particles goes like t^2 for short times (ballistic regime) and is proportional to t in the long-time diffusion limit. When stable background stratification is present, dispersion in the vertical direction is suppressed. As a result, a plateau is found for single-particle dispersion in the vertical direction, which scales proportional to N^{-2} with N the buoyancy frequency.[1,2] This plateau is reached for intermediate times, around $t=2\pi/N$. In the present work, this plateau is found too, but moreover we find a diffusive regime for long times. The effect of stratification on horizontal dispersion is not clear yet, often it is assumed to be similar to dispersion in homogeneous isotropic turbulence.[1,2,16] Liechtenstein *et al.*[4] find a long-time behavior that is proportional to t^2 when using the linear RDT model, whereas their DNS results show a slight tendency toward a diffusive regime. Our work, resulting from long time series of statistically stationary stratified turbulence, shows a clear superdiffusive regime for long-time horizontal dispersion, which is proportional to t^α with $\alpha=2.1\pm0.1$.

Attempts to model single-particle dispersion in stratified flows started with the work of Csanady.[17] More recently, next to the above-mentioned plateau, a theoretical model by Pearson *et al.*[5] predicts a linear growth of the mean-squared vertical displacement for large times.

For particle-pair dispersion, the theoretical scaling laws for isotropic turbulence depend on the initial separation between the particles.[18,19] When stratified turbulence is considered, vertical dispersion is suppressed as for single-particle statistics. Nicolleau and Vassilicos[2] retrieved a plateau again at $t\simeq 2\pi/N$ and observed the beginning of a second plateau for large times. These two regimes and a final diffusive regime have been retrieved in the present study. Horizontal pair dispersion shows three regimes, as in isotropic turbulence. Initially, the classical ballistic regime is obtained, followed by a larger slope in the intermediate range and again a smaller slope for long times. For long times, the particles are expected to become uncorrelated, resulting in similar long-time dispersion behavior for single particles and particle pairs. Nicolleau and Vassilicos[2] indeed found this behavior, with a scaling that is proportional to t. Liechtenstein *et al.*[4] see a much stronger final growth, which according to them is most likely caused by too short integration times.

To study the shape of a cloud of particles, the evolution of a group of particles—four in this work—can be followed. Experimentally, Lagrangian measurements of a cluster of particles can be used to derive the full set of spatial velocity derivatives, useful, for example, to study vorticity dynamics.[20] Lagrangian multiparticle statistics are described in homogeneous isotropic turbulence by Pumir *et al.*[21] and Biferale *et al.*[22] They found that particle clusters with an initial tetrahedral shape were strongly distorted and tended to become elongated, almost coplanar objects. It will be elucidated in this work that the shape of a group of particles is flatter and more elongated in stratified turbulence compared to isotropic turbulence.

The numerical method used in this work is introduced in Sec. II. Next, in Sec. III, the type of flow resulting from numerical simulations of forced stably stratified turbulence will be described and a validation of the forcing method is given. Thereafter, results are discussed in Sec. IV for both horizontal and vertical dispersion of single particles, particle pairs, and tetrads.

II. NUMERICAL METHOD

A. DNS of the Boussinesq equations

The motion of an incompressible fluid in a stably stratified environment is fully described by the Navier–Stokes equations in combination with an equation that imposes the divergence-free constraint and one for the density. After applying the Boussinesq approximation and using the hydrostatic balance $\partial\bar{p}/\partial z=-(\rho_0+\bar{\rho})g$, they can be written as

$$\nabla\cdot\boldsymbol{u}=0, \tag{1}$$

$$\frac{\partial\boldsymbol{u}}{\partial t}+\boldsymbol{u}\cdot\nabla\boldsymbol{u}=-\frac{1}{\rho_0}\nabla p'-\frac{\rho'}{\rho_0}g\hat{\boldsymbol{z}}+\boldsymbol{F}_{u,\mathrm{ext}}+\nu\nabla^2\boldsymbol{u}, \tag{2}$$

$$\frac{\partial\rho'}{\partial t}+\boldsymbol{u}\cdot\nabla\rho'=wN^2\frac{\rho_0}{g}+\kappa\nabla^2\rho'. \tag{3}$$

Herein is $\boldsymbol{u}=(u,v,w)$ the velocity in the x, y, and z direction, respectively, with $\hat{\boldsymbol{z}}$ pointing upwards. Furthermore, ρ is the density, p is the pressure, g is the gravitational acceleration, ν is the molecular viscosity, and κ is the scalar diffusivity. $\boldsymbol{F}_{u,\mathrm{ext}}$ represents the external forcing. The buoyancy frequency, or Brunt–Väisälä frequency, is defined as $N^2=(-g/\rho_0)\partial\bar{\rho}/\partial z$ and the ratio of $\nu/\kappa=\mathrm{Sc}$ is the Schmidt number. The density $\rho=\rho_0+\bar{\rho}(z)+\rho'(x,y,z,t)$ is split in three components: a typical value (ρ_0) plus a time-independent linear background profile $(\bar{\rho})$ plus a fluctuating part (ρ'). The choice of a linear background implies a homogeneous stratification. Fluctuating components are indicated with a prime, and in the following an overbar is used for an averaged quantity. For properties of the flow field, this average is a spatial average over the computational domain, whereas Lagrangian statistics are calculated from ensemble averages over all particles. Note that in taking both averages, we used homogeneity in both horizontal and vertical directions.

The equations of motion are solved using a three-dimensional parallel pseudospectral DNS code (see Ref. 23 for details). DNS enables us to solve the Navier–Stokes equations exactly at all relevant scales in the flow without making use of any model. The main drawback is that only

TABLE I. Properties of the different simulations presented in this work. Cases N0–N1000 are runs with increasing stratification strength, performed at a resolution of 128^3 with Sc=1. For a buoyancy frequency $N=0.98\ s^{-1}$, simulations are run in which some parameters are changed. For cases Sc=0.5, Sc=2, and Sc=7, the Schmidt number is modified; case 256^3 is run at a higher resolution of 256^3; in case horF forcing is applied in horizontal direction only; and in case lowF the forcing amplitude is reduced.

Case	N (s^{-1})	Fr_z	Fr_h	Re_h	u_h/u_{rms}	u_z/u_{rms}	L_z/L_h	$k_{\max}\eta$
N0	0	—	—	205	1.0	1.0	1.0	1.2
N1	0.098	0.89	0.58	235	1.06	0.86	0.65	1.4
N10	0.309	0.22	0.09	553	1.19	0.40	0.39	1.8
N100	0.98	0.09	0.03	618	1.22	0.36	0.32	1.7
N1000	3.09	0.05	0.01	731	1.25	0.36	0.24	1.4
Sc=0.5	0.98	0.09	0.03	613	1.23	0.35	0.32	1.7
Sc=2	0.98	0.10	0.03	624	1.20	0.37	0.31	1.6
Sc=7	0.98	0.11	0.03	608	1.22	0.39	0.29	1.6
256^3	0.98	0.12	0.04	1148	1.16	0.49	0.32	1.7
horF	0.98	0.44	0.04	546	1.22	0.15	0.09	1.3
lowF	0.98	0.08	0.02	455	1.21	0.26	0.27	2.1

relatively low resolutions can be used, thus flows with relatively low Reynolds numbers can be solved due to its high computational costs. The results presented here are derived from simulations with a resolution of 128^3 to be able to track particles for very long times. However, as a check most cases are studied also at a higher resolution (256^3) and they gave similar results for the time range that could be resolved at that resolution. One of these higher-resolution results is included in Fig. 2 as a demonstration. A cubic domain of width $L_0=1$ is used. Periodic boundaries are implemented in all three directions, allowing the use of a Fourier representation of the velocity and scalar field. Time-stepping of the linear viscous term is performed using exact integration, whereas the other terms are treated by a third-order Adams–Bashforth method.

In a precomputation, a divergence-free homogeneous isotropic turbulent velocity field is created using forcing of the flow by injecting energy at the largest scales, equally in all three directions. A general description of the forcing scheme is

$$F^{n+1}(\boldsymbol{k}) = (1-\alpha)F^n(\boldsymbol{k}) + AR(\boldsymbol{k})e^{i\phi(\boldsymbol{k})}, \tag{4}$$

where $(1-\alpha)F^n$ (with $\alpha=[0,1]$) denotes a memory effect of the forcing. A is the forcing amplitude, R is a random value for the forcing amplitude taken from a Gaussian with zero mean and standard deviation 1, and ϕ adds a random phase to every forced wavenumber mode. R and ϕ have different values for each forced wavenumber and at each forcing time. F^{n+1} and F^n are the forces at forcing times $n+1$ and n, respectively. The value of the force is updated every m time step (forcing time $t_f=m\Delta t$) with $m=\mathcal{O}(5-10)$. Forcing is only applied to the largest scales of the velocity field with wavenumber modes $0<k\leqslant 2\sqrt{2}k_0$ ($k_0=2\pi/L_0$ the smallest wavenumber), and serves to keep the total kinetic energy statistically stationary. Here $k=\|\boldsymbol{k}\|$ is the length of the wavenumber vector $\boldsymbol{k}=(k_x,k_y,k_z)$ in which wavenumber k_i, with $i\in\{x,y,z\}$, is a multiple of k_0.

The initial conditions of the simulations of forced homogeneously stratified turbulence are a velocity field of homogeneous isotropic turbulence together with a zero-valued scalar fluctuation field. At $t=0$, a linear stable background stratification is switched on by assigning a nonzero value to N, which is kept constant throughout the simulation. Four different levels of the background stratification are studied, whereby N^2 is varied by a factor of 10 between the different cases. Furthermore, a simulation of homogeneous isotropic turbulence is run in which $N=0\ s^{-1}$. The forcing method mentioned above is used of which the amplitude A and the forcing time t_f are adapted to keep the kinetic energy statistically stationary. The amplitude A is chosen as high as allowed by the requirement of stationarity, to reach the highest possible Reynolds numbers. Some properties of the different runs are given in Table I.

In order to check whether forcing with equal strength in all three directions is allowed for the resulting anisotropic flow, we also performed a simulation in which only wavenumber modes in the range mentioned above and with $k_z=0$ are forced (case horF). In this way, inducing vertical fluid motion by the artificial forcing is avoided; velocity fluctuations in vertical direction are only created via nonlinear interaction with the horizontal velocity components. The relative importance of stratification can be expressed by the vertical Froude number, which is defined here as $\mathrm{Fr}_z=u_{\mathrm{rms}}/NL_z$, and it gives the ratio of inertial forces to buoyancy forces. The root-mean-squared velocity is given by $u_{\mathrm{rms}}^2=\frac{2}{3}E_{\mathrm{kin}}$ and L_z is the vertical integral length scale given by $\int_0^\infty R_{ww}(z)dz$, with $R_{ww}(z)$ the Eulerian spatial velocity autocorrelation function in vertical direction. The total kinetic energy per unit mass, E_{kin}, is calculated as $E_{\mathrm{kin}}=\frac{1}{2}(u'^2+v'^2+w'^2)=2E_h+E_z$. The results in the horizontal directions x and y do not significantly differ (within 3% for the rms velocities and length scales) and therefore in the following only the averaged horizontal values will be used. An impression of the degree of anisotropy of the flow can be derived from the ratios u_h/u_{rms}, u_z/u_{rms}, and L_z/L_h. The horizontal velocity u_h is calculated from the total energy E_h in horizontal direction and similarly the vertical velocity u_z stems from the

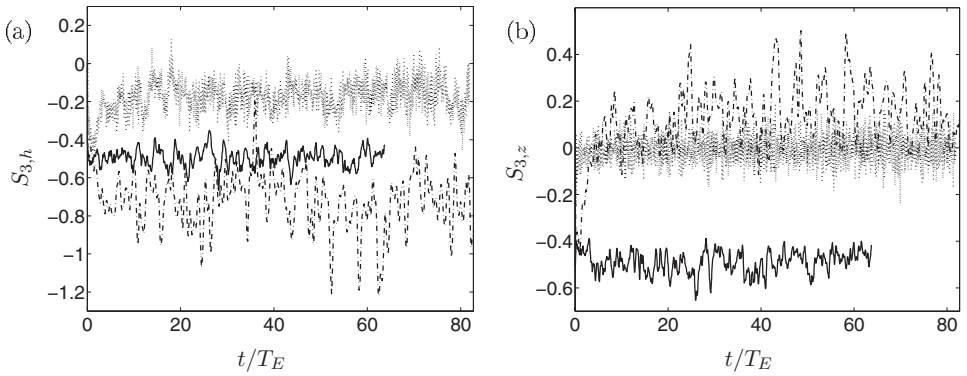

FIG. 1. Horizontal (a) and vertical (b) velocity derivative skewness as function of time for three values of the stratification: N0 (—), N10 (– · – · –), N1000 (···). For clarity, cases N1 and N100 are left out. They show similar quasisteady behavior around values of −0.52 and −0.37 (horizontal) and −0.43 and 0.02 (vertical), respectively.

vertical kinetic energy E_z. For the calculation of the horizontal length scale, a similar formula is used as mentioned above for the vertical length scale, thereby taking the averaged value of the components in the x and y directions. The values for $k_{\max}\eta$, with $k_{\max}$ the highest wavenumber resolved by the grid and η the Kolmogorov length scale, are included in the table as a measure for the resolution. For a well-resolved simulation, it is required that $k_{\max}\eta > 1$.[11] A measure for the turbulence intensity is $\mathrm{Re}_\lambda \approx 85$ for the initial velocity field. Here the Reynolds number $\mathrm{Re}_\lambda = u_{\mathrm{rms}}\lambda/\nu$ with length scale $\lambda = \sqrt{\overline{u'^2}/\overline{(\partial u'/\partial x)^2}}$. Most of the results shown in this work are derived from simulations where $\mathrm{Sc}=1$. For one value of the stratification (case N100), simulations are run with different Schmidt numbers ($\mathrm{Sc}=0.5,1,2,7$) to study the influence of Sc on particle dispersion.

B. Particle tracking

A natural way to describe turbulent dispersion is the Lagrangian frame of reference, in which the observer is moving with the particle. Here we study fluid particles, which are infinitely small fluid elements that exactly follow the flow. Particle trajectories are derived from

$$\frac{d\boldsymbol{x}_p}{dt} = \boldsymbol{u}_p, \tag{5}$$

with $\boldsymbol{x}_p$ the particle position and $\boldsymbol{u}_p = \boldsymbol{u}(\boldsymbol{x}_p)$ its velocity. The velocity at the particle position can be derived from knowledge of the Eulerian velocity field by use of interpolation. Cubic spline interpolation of the velocity field at the particle position is implemented in the code. Next, the particle trajectories are obtained by numerical integration of Eq. (5). Time integration is performed using the same third-order Adams–Bashforth technique as for the Eulerian velocity field.

Velocity and position time series of 16384 particles are collected for about 50 eddy turnover times $T_E = L_h/u_{\mathrm{rms}}$. These particles are grouped in triangular pyramid structures, to be able to study both single-particle and particle-pair statistics and the evolution of tetrads. The initial position of one-quarter of the particles is uniformly spread over the computational domain. The other particles are initially located at a fixed separation (about $\frac{5}{2}\eta$ for cases N1, N10, and N100) in the x, y, and z directions from the reference particles. For two values of the background stratification (cases N0 and N1000), the influence of the initial particle separation on particle-pair and multiparticle statistics is also studied. In these cases, 81920 particles are tracked with initial separations of about $\frac{1}{6}$, $\frac{3}{4}$, $\frac{3}{2}$, 6, and 15 (in units of η) in all three directions. Particles are released when the flow has reached a quasi-stationary state.

III. FLOW STRUCTURE IN FORCED STRATIFIED TURBULENCE

A. Validation of the forcing method

An important question in this work is whether it is possible to maintain a state of statistically stationary stably stratified turbulence by applying artificial forcing. If energy transfer to smaller scales is modified or an inverse cascade is present in the flow, forcing of the large scales could lead to accumulation of energy at these scales and eventually to a collapse of the simulation. We do find that the type of forcing described in Sec. II A with equal strength in all three directions results in a quasi-stationary state. Checking stationarity is done by looking both at kinetic energy in all three directions and at the velocity derivative skewness S_3. The velocity derivative skewness is defined as

$$S_{3,z} = \frac{\overline{(\partial w'/\partial z)^3}}{\overline{(\partial w'/\partial z)^2}^{3/2}} \tag{6}$$

for the vertical component, and in an analogous way for the horizontal component, $S_{3,h}$. Time series of $S_{3,h}$ and $S_{3,z}$ are shown in Fig. 1 and their time-averaged values are given in Table II. The value of these quantities for case N0 (−0.49) is

TABLE II. Averaged values with standard deviation of the skewness S_3 and flatness factors K for the five cases, calculated according to Eqs. (6) and (8). Distinction is made between the horizontal and the vertical component. Standard deviations are largest for cases N10 and N100, which were the most difficult to get completely stationary.

Case	$S_{3,h}$	$S_{3,z}$	K_h	K_z
N0	-0.49 ± 0.05	-0.49 ± 0.05	4.7 ± 0.3	4.7 ± 0.2
N1	-0.52 ± 0.06	-0.43 ± 0.05	4.8 ± 0.3	4.5 ± 0.2
N10	-0.72 ± 0.15	0.13 ± 0.14	6.3 ± 1.1	5.2 ± 0.7
N100	-0.37 ± 0.11	0.02 ± 0.08	3.8 ± 0.5	3.6 ± 0.3
N1000	-0.18 ± 0.08	0.01 ± 0.06	3.3 ± 0.2	3.2 ± 0.2

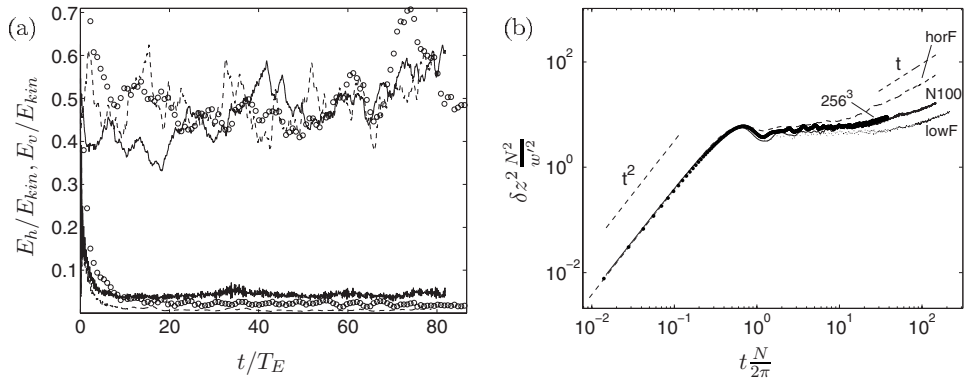

FIG. 2. (a) Horizontal (topmost lines) and vertical kinetic energy as a function of time. The gap between horizontal and vertical kinetic energy is slightly larger for purely horizontal forcing (dashed lines) than for equal forcing strength in all three directions (solid line for high-energy run, open circles for low-energy run). Graphs are made dimensionless with the time-averaged total kinetic energy of the different runs. (b) Vertical single-particle mean-squared displacement as function of time for horizontal forcing (dashed line) and three-dimensional forcing [128^3: — (high energetic), ⋯ (low energetic), 256^3: ●]. The stratification for both plots is $N=0.98\ s^{-1}$. See Sec. IV A for a discussion on the apparent difference in long-time dispersion behavior between 2D and 3D forcing.

consistent with values found in studies of homogeneous isotropic turbulence. In isotropic turbulence, a negative value of S_3 points to a forward energy cascade.[24] Whether this relation holds for stratified turbulence is unknown. For all cases studied in this work, the skewness S_3 fluctuates around constant values, demonstrating the statistically stationary state reached in the simulations. With increasing stratification, the value of $S_{3,h}$ first becomes more negative and then goes toward zero, whereas $S_{3,z}$ first increases—even becomes positive—and then decreases also toward zero. This trend is also visible in Fig. 1 of the work by Kimura and Herring.[1] The behavior of the skewness for moderate stratification [case N1 (not shown) and mainly case N10] might be explained by a dominance of the effect of anisotropy of the flow on nonlinear energy transfer. For strong stratification [cases N100 (not shown) and N1000], the velocity derivative skewness goes toward zero, indicating suppressed nonlinear energy transfer from small to large wavenumbers.

Two convincing indications for the existence of a forward energy cascade in forced stably stratified turbulence are found. No accumulation of energy takes places at the largest scales in the flow, which would give a blowup of the total kinetic energy. Moreover, a test in which forcing is applied around $k=8k_0$ resulted in a flow with only a little amount of energy at the largest scales (smallest wavenumbers k), displaying only small-scale flow structures. Because of the presence of this clear forward energy cascade, large-scale forcing as applied in this study is appropriate.

A big advantage of performing forced stratified turbulence simulations for dispersion studies is the following. By keeping the energy distribution over the length scales in the flow statistically stationary, the turbulence level is kept constant and hence the relative importance of the background stratification with respect to turbulence (quantified by the Richardson number, see Sec. III B) remains constant. This is not the case for decaying stratified turbulence. The energy spectra of decaying stratified turbulence simulations progressively steepen in the course of time due to dissipation at the smallest scales, thereby increasing the relative importance of the background stratification.

In Fig. 2, the horizontal and vertical kinetic energy are shown as a function of time for a stratification with $N=0.98\ s^{-1}$. Three runs are shown, one with purely horizontal forcing (case horF) and two with 3D forcing (cases N100 and lowF). The difference between these last two runs is the amount of energy that is added to the flow by the forcing (total kinetic energy differs by a factor of about 2). Cases N10 and N100, where the strongest competition is to be expected between turbulence generation by forcing on the one hand and turbulence suppression due to stratification on the other hand, were most difficult to get completely stationary. A slight increase in time of the averaged horizontal kinetic energy time is found (for example, solid line in Fig. 2). A completely flat horizontal kinetic energy level is only achieved when the applied forcing amplitude was small, and the flow could hardly be called turbulent. In terms of kinetic energy, for case lowF it follows from the energy spectra that only approximately 1% (compared to 10% for isotropic turbulence and 3–4% for case N100) of the energy is found at $k/k_0>10$, so almost all small-scale motion has then vanished. The slight increase in the kinetic energy is probably caused by the excitation of internal gravity waves, as discussed by Lindborg and Brethouwer.[25] However, the particle dispersion (mean-squared displacement) in both high (case N100) and low (case lowF) energetic stratified flows is very similar. In particular, the scaling behavior in the different time regimes shows few differences with energy level. For vertical dispersion, this is shown in Fig. 2(b), and also for horizontal dispersion the slopes for both short times and long times are approximately the same for both runs. The results shown in this work are derived from the high energetic case in which the horizontal kinetic energy increases slightly. This choice is based on the following argument. For comparison of the cases N10 and N100 with cases N1 and N1000, where

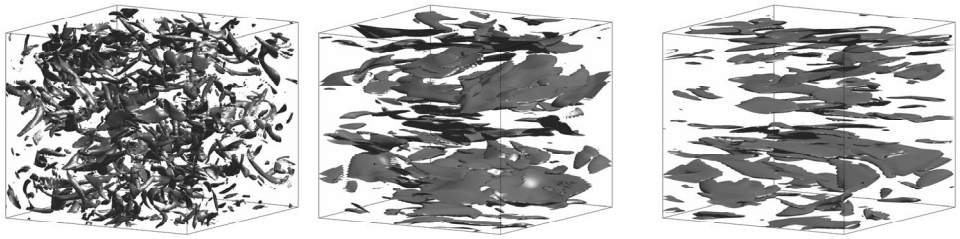

FIG. 3. Isovorticity surfaces of cases (a) N1 at $2.0\omega_{\mathrm{rms}}$, (b) N10 at $1.6\omega_{\mathrm{rms}}$, and (c) N100 at $1.6\omega_{\mathrm{rms}}$. With increasing stratification, the structures become more horizontal and "pancake-like" and fewer small-scale structures are visible.

it was easy to obtain quasistationarity, a comparable amount of small-scale motion is preferred, thereby avoiding a too short range of length scales in the flow.

Furthermore, (an)isotropy of the forcing is tested, because the resulting flow is anisotropic for cases with $N \neq 0$. Applying equal forcing in all three directions or purely forcing the horizontal wavenumber modes leads to different flow configurations, with the main differences being the ratio between the vertical and horizontal kinetic energy (see Fig. 2(a)) and the ratio L_z/L_h (0.32 for 3D forcing, 0.09 for horizontal forcing). Dispersion statistics, however, are qualitatively very similar despite differences in the large-scale flow structures. For the vertical direction, dispersion statistics are shown in Fig. 2(b) for both purely horizontal and three-dimensional forcing (both high and low energetic), as well as for a simulation performed with 3D forcing at higher resolution (256^3). For horizontal dispersion (not shown), the differences between the two forcing methods (2D and 3D) are hardly visible and the slopes are exactly the same. A detailed description of the results follows in Sec. IV A; for now only the strong resemblance between the two forcing methods is of importance. Horizontal forcing cannot be applied to the isotropic case N0 and the weakly stratified case N1. In order to make all simulations comparable, the same forcing type, and thus 3D, is chosen.

B. Flow structure and density profile

To get an idea of the structures in the flow, in Fig. 3 plots of isovorticity surfaces for different stratification levels are shown. The isovorticity surface of case N1 resembles those found for 3D isotropic turbulence; the structures are small and directed in all three directions. The strong stratification (case N100) shows the "well-known" pancake-like structures, whereas for the weaker stratification (case N10) traces of small-scale structures can be seen in addition to the pancakes. The pancake-like structures are related to regions of strong vertical shear.[1] In Fig. 4, the horizontally averaged square of the vertical shear, defined as

$$\Sigma^2 = \left\langle \left(\frac{\partial u}{\partial z}\right)^2 + \left(\frac{\partial v}{\partial z}\right)^2 \right\rangle_h, \tag{7}$$

is plotted as a function of z for case N100. Alternating regions of high and low vertical shear demonstrate the layered structure. According to Brethouwer *et al.*,[26] the dynamics of turbulence affected by stable stratification can be classified into two distinct regimes. As in the work by Billant and Chomaz,[27] they introduce a parameter $R = \mathrm{Re}_h \mathrm{Fr}_h^2$, with $\mathrm{Re}_h = u_{\mathrm{rms}} L_h/\nu$ the horizontal Reynolds number and $\mathrm{Fr}_h = u_{\mathrm{rms}}/L_h N$ the horizontal Froude number. For $R < 1$, large smooth horizontal layers can be observed and energy is dissipated mainly by vertical shearing of the large-scale pancake-like structures. When $R > 1$, large quasihorizontal layers are still noticeable but at the same time small-scale turbulentlike motions are present and dissipation takes place predominantly at these smallest scales. For the cases studied in the present work, this classification would separate cases N1 and N10 ($R > 1$) from cases N100 and N1000 ($R < 1$). For case N1, the effect of stratification is only weak, but for case N10 in Fig. 3 indeed large-scale horizontal structures can be already identified in combination with small-scale fluctuations. According to Brethouwer *et al.*,[26] these small-scale motions are most likely due to Kelvin–Helmholtz-type instabilities generated by shear between different layers. The fact that case N10 reveals both large-scale horizontal structures and appreciable small-scale fluctuations, thus representing highly anisotropic turbulent flow, explains the abnormal values of the skewness ($S_{3,h} \approx -0.72$ and $S_{3,z} \approx +0.13$; see Sec. III A) and the flatness (see below). The influence of large-scale dissipation for cases N100 and N1000, resulting in reduced transport of energy through a cascading process, becomes clear also from the values of the velocity derivative skewness (see Fig. 1).

In a similar fashion as for the skewness, which gives a measure of the asymmetry of a probability density function

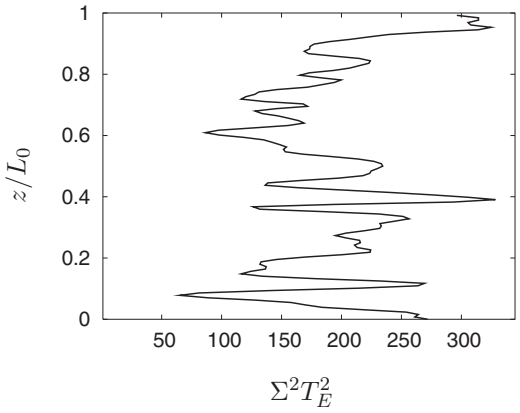

FIG. 4. Mean-squared shear for case N100 as a function of vertical position z at a single moment in time. A layered structure is seen with regions of high and low shear.

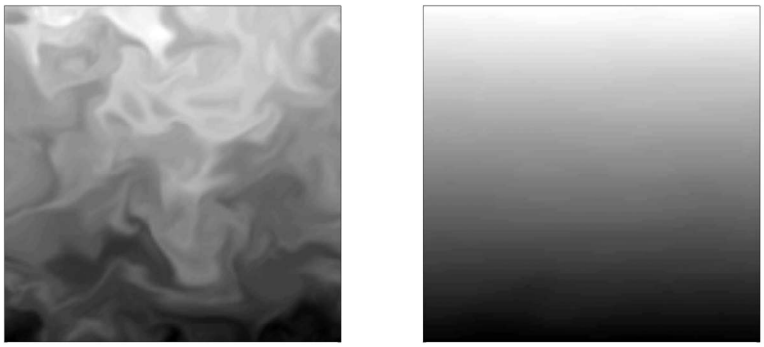

FIG. 5. Vertical cross sections of the density profile. For case N1 (a) mixing is clearly visible, whereas case N100 (b) only shows slight fluctuations upon the linear background profile.

(pdf) of the velocity derivatives, the flatness factor—or kurtosis—can be defined from the fourth-order moment according to

$$K_z = \frac{\overline{(\partial w'/\partial z)^4}}{\overline{(\partial w'/\partial z)^2}^2} \tag{8}$$

for the vertical component and analogous for the horizontal component K_h. This factor gives a measure of the width of the tails of the velocity derivative pdf, and as such an impression of the intermittency present in a flow. For a normal distribution this value is 3 (no intermittency) and higher flatness factors are associated with a certain level of intermittency. In the cases studied in this work, the flatness factor is quasisteady in time and its values are given in Table II. It can be seen that with increasing stratification, the flatness factor decreases, with an exception for case N10, and so the flow shows less intermittent behavior. Furthermore, again a distinction is notable between cases N1 and N10 on the one hand and cases N100 and N1000 on the other hand. The first two show anisotropy in the values of the flatness factor, whereas the second two have similar values for both horizontal and vertical directions.

Also vertical cross sections of the density profile clarify the processes occurring in stably stratified turbulence. They are given in Fig. 5 for two different values of the background stratification. Figure 5(b) shows an almost linear density profile. There the stable stratification is so strong that turbulent fluctuations are hardly visible. For moderate stratification [Fig. 5(a)], much more overturning and mixing between different layers can be seen. To quantify the amount of mixing, a local gradient Richardson number can be defined as

$$\mathrm{Ri}_g = \frac{N^2}{\left(\frac{\partial u_h'}{\partial z}\right)^2}, \tag{9}$$

which is a ratio of restoring buoyancy forces and turbulence producing shear forces. Here u_h' is the horizontal component of the fluctuating velocity field at a single moment in time. For steady mean shear flows of an inviscid stably stratified fluid, the Miles–Howard criterion states that the flow can only be unstable and turbulent when $\mathrm{Ri}_g < \mathrm{Ri}_{cr} = 0.25$. For practical flow situations different values are found, all of order $\mathcal{O}(1)$.[28] Probability density functions of the values of Ri_g in the whole computational domain at a single time step are shown for different values of the stratification in Fig. 6, including the reference value 0.25. For case N1, it can be seen that in large parts of the domain, shear effects are dominant ($\mathrm{Ri}_g < 1$ at about 60% of the gridpoints), so a lot of overturning is possible. This picture changes considerably with increasing stratification. For case N10, about 25% of the gridpoints has $\mathrm{Ri}_g < 1$, and for case N100 this is $\approx 0\%$; almost all mixing has vanished there.

Wavelike motion is present in both the velocity and the scalar field. It can be seen in most quantities (Eulerian and

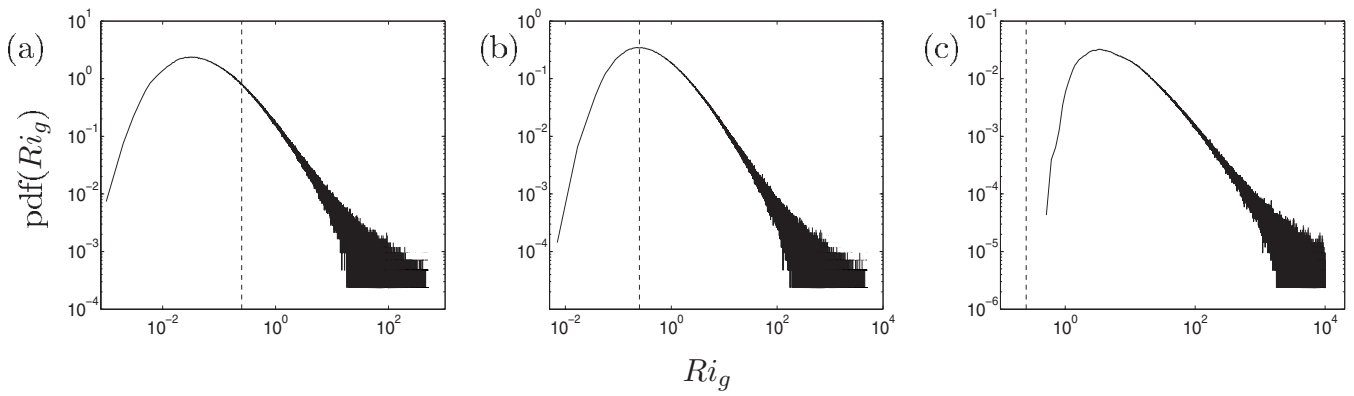

FIG. 6. Probability density functions of the gradient Richardson number for cases N1, N10, and N100, respectively. The theoretical critical value of $\mathrm{Ri}_{cr} = 0.25$ is also shown in the graphs (dashed line). With increasing stratification, less turbulent overturning can take place.

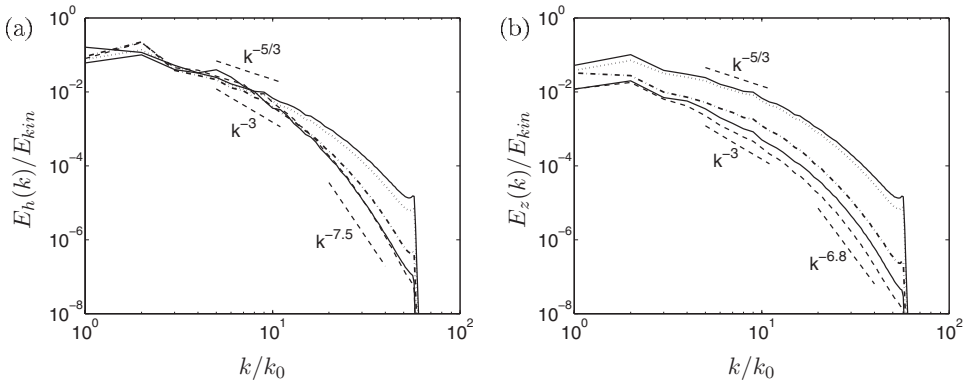

FIG. 7. Horizontal (a) and vertical (b) energy spectra, calculated according to Eqs. (10) and (11), respectively, as a function of k/k_0 for different stratification levels; N0 (—), N1 (···), N10 (– · – · –), N100 (----), N1000 (—).

Lagrangian, mainly in the vertical) for which the evolution in time is studied, such as kinetic and potential energy, length scales, autocorrelation functions, and particle dispersion; see, for example, the oscillations around the plateau in Fig. 8(b). The frequency of these waves corresponds to the buoyancy frequency, their fundamental frequency $f \simeq N$.

The energy distribution between different length scales in the flow is different in stratified turbulence compared to isotropic turbulence. This becomes clear from the energy spectra plotted in Fig. 7. They are calculated as

$$E_h(k_i) = \sum_{k_i-\frac{1}{2}k_0 \le k < k_i+\frac{1}{2}k_0} \frac{1}{2}(|\hat{u}(k)|^2 + |\hat{v}(k)|^2), \tag{10}$$

$$E_v(k_i) = \sum_{k_i-\frac{1}{2}k_0 \le k < k_i+\frac{1}{2}k_0} \frac{1}{2}|\hat{w}(k)|^2 \tag{11}$$

for horizontal and vertical directions, respectively. For the isotropic case, a small region with inertial range scaling ($k^{-5/3}$) can be seen. The influence of stratification on the flow for the weakest stratified case N1 is rather small, as its spectra have almost the same shape as in isotropic turbulence (case N0). All three stronger stratified cases show qualitatively the same behavior. Both in horizontal and vertical direction, the spectrum becomes steeper for stratified turbulence, so less energy is present at the smallest scales. Comparing the horizontal and vertical directions [see Figs. 7(a) and 7(b), respectively], at the largest scales much more energy can be found in the horizontal velocity components than in the vertical velocity component. The horizontal spectrum, however, falls off faster at higher wavenumbers.

The flow is highly anisotropic for the strongest stratified cases, as can be deducted, for example, from the values of the ratios u_h/u_{rms}, u_z/u_{rms}, and L_z/L_h in Table I. The vertical length scale L_z gives a measure of the layer thickness and the horizontal length scale L_h can be interpreted as the width of the energy-containing eddies. The ratio L_z/L_h decreases with increasing stratification because both L_z decreases and L_h increases. To check whether the growth of the horizontal length scales is not limited by the size of the domain or becomes too large to be able to use periodic boundaries (L_h should be smaller than $0.5L_0$), a simulation is performed with horizontal domain size $2L_0$. The results of this simulation do not show marked differences in both L_h and the dispersion behavior of fluid particles.

IV. PARTICLE DISPERSION IN FORCED STRATIFIED TURBULENCE

A. Single-particle dispersion

The dispersion—or mean-squared displacement—of particles is given by Taylor's equation,

$$\overline{(X(t)-X(0))^2} = 2u_{\mathrm{rms}}^2 \int_0^t (t-\tau)R_L(\tau)d\tau \tag{12}$$

under the assumption that the Lagrangian and Eulerian rms velocities are the same $\left(u_{\mathrm{rms}}^2 = \frac{2}{3}E_{\mathrm{kin}}\right)$ and that the flow is homogeneous and stationary. $R_L(\tau)$ is the Lagrangian velocity autocorrelation function, which is only a function of the time separation $\tau = t - t'$,

$$R_L(\tau) = \frac{\overline{u_p'(t')u_p'(t)}}{u_{\mathrm{rms}}^2}. \tag{13}$$

Using the known properties of the autocorrelation function, $R_L(0)=1$ and $T_L = \int_0^\infty R_L(\tau)d\tau$ with T_L the Lagrangian time scale, the following relations can be derived for dispersion in homogeneous isotropic turbulence:

$$\overline{(X(t)-X(0))^2} \approx u_{\mathrm{rms}}^2 t^2, \quad t \to 0, \tag{14}$$

$$\overline{(X(t)-X(0))^2} \approx 2u_{\mathrm{rms}}^2 T_L t, \quad t \to \infty \tag{15}$$

(see standard textbooks on turbulence for a derivation of the above equations, for example, Refs. 24 and 29). In the following, T_L for case N0 will be used as a typical Lagrangian time scale. For case N0, the ratio of the Lagrangian time scale and the Eulerian time scale $T_E = L_h/u_{\mathrm{rms}}$ is $T_L/T_E \approx 0.7$, consistent with values found in literature.[19] This ratio decreases with increasing stratification because the typical time scale of the flow T_E increases. For stratified turbulence, several authors (see, for example, Refs. 2, 5, and 30) provided evidence of a plateau for vertical dispersion for $t \gtrsim 2\pi/N$. This plateau scales as

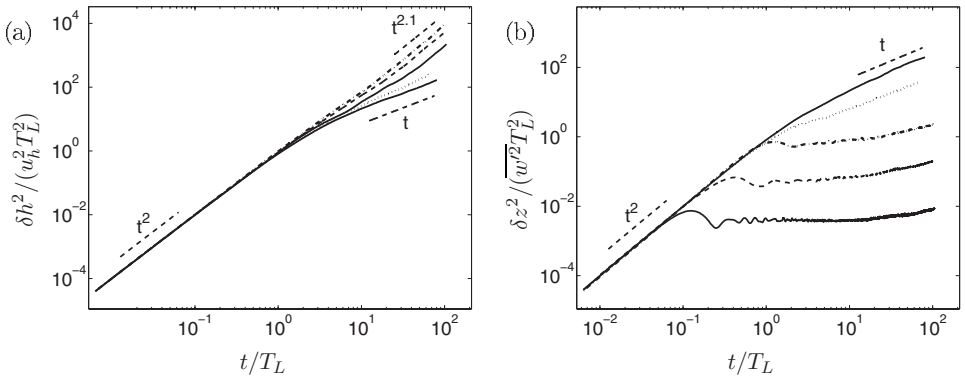

FIG. 8. Horizontal (a) and vertical (b) single-particle dispersion as a function of time for five different cases: N0 (—), N1 (···), N10 (– · – · –), N100 (----), N1000 (—). The plateau for vertical dispersion starts around $t=2\pi/N$.

$$\overline{(Z(t)-Z(0))^2} \approx \frac{\overline{w'^2}}{N^2}. \tag{16}$$

Furthermore, the choice of the rms velocity in Eq. (16) differs; some take the overall value as defined in Sec. II A,[2] while others use only the component in vertical direction.[5] We use the vertical component given by $\overline{w'^2}=2E_z$ with E_z the kinetic energy in vertical direction. In the following, horizontal dispersion $\frac{1}{2}(\overline{(X(t)-X(0))^2}+\overline{(Y(t)-Y(0))^2})$ will be denoted by δh^2 and for the vertical direction $\delta z^2 = \overline{(Z(t)-Z(0))^2}$ will be used.

As described in the Introduction, horizontal dispersion in stratified turbulence is often assumed to be similar to that in homogeneous isotropic turbulence. Only recently, some first doubts about this assumption have been put forward by Liechtenstein *et al.*[4] From their work, however, it cannot be deduced whether the superdiffusive long-time regime is inherent to the type of flow under consideration or that it is a result of too short integration times.

Single-particle dispersion in horizontal and vertical directions in stationary stratified turbulence is shown in Fig. 8 for five different values of the density stratification. For isotropic turbulence (case N0), we do retrieve the classical regimes of Eqs. (14) and (15), as well as for horizontal dispersion in relatively weak stratification (case N1). For strong stratification, the plateau with its accompanying scaling is found for vertical dispersion. When the horizontal and vertical axes of Fig. 8(b) are rescaled to $tN/2\pi$ and $\delta z^2 N^2/\overline{w'^2}$, respectively, the onset of the plateaus collapse, as can be seen in Fig. 9(a). For times up to about $t/T_L=\mathcal{O}(10)$, these plots resemble the results of Refs. 1 and 2.

For longer times a new regime can be identified, which becomes available by tracking the particles for sufficiently long times in a quasi-stationary stably stratified flow. Dispersion in vertical direction starts to increase again and is proportional to t, which is a clear indication of a diffusion process. This diffusion of fluid particles away from the original equilibrium position is caused by molecular diffusion of the active scalar (density), which we checked by changing the Schmidt number. The effect of the Schmidt number on dispersion in vertical direction is shown in Fig. 9(b). With increasing Sc, or similarly with decreasing molecular diffusion of the density, vertical dispersion indeed reduces; the diffusive regime sets in at later times. In the limit of $\mathrm{Sc}\to\infty$ ($\kappa\downarrow 0$), only the plateau would be found. The diffusive regime was already predicted by the model of Pearson *et al.*[5] From their work, it can be deduced that the time scale for the fluid elements to change their density (τ_{trans}) is proportional to the Schmidt number, $\tau_{\mathrm{trans}}\propto \mathrm{Sc}$. Here we choose this starting time of the diffusive regime as the point at which vertical single-particle dispersion starts to deviate from the results for case Sc=7. It is found that these starting times τ_{trans} double when Sc doubles from 0.5 to 1 and from 1 to 2, thereby confirming in this range of Schmidt numbers the predictions made by Pearson *et al.*[5] This scaling regime has not been observed in decaying stratified turbulence. In the available

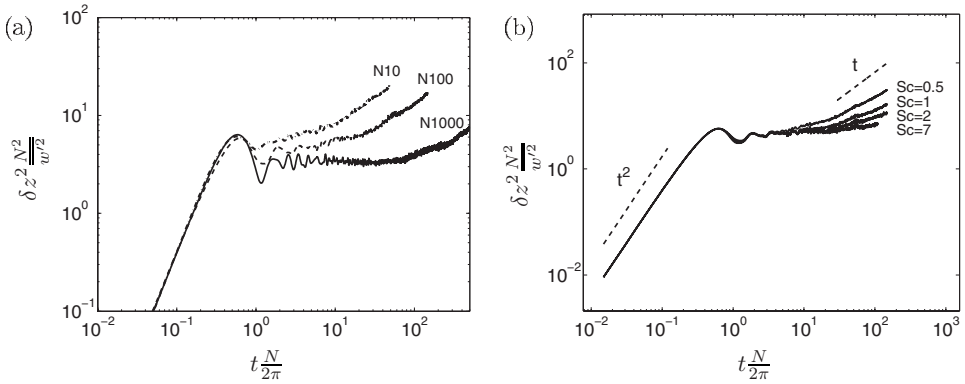

FIG. 9. (a) Same plot as Fig. 8(b) for cases N10–N1000. The axes are rescaled to elucidate the scaling behavior and the collapse of the onset of the plateaus. (b) Vertical dispersion for case N100 for different values of the Schmidt number Sc. With increasing Sc (or similarly decreasing molecular diffusion), the onset to long-time diffusion is delayed, clarifying the role of molecular diffusion in vertical particle dispersion.

studies,[1,3,4] the energy content of the turbulent flow reduces too fast in the course of time to enable observation of this regime.

The following observations are made for vertical dispersion. In the early stages, particles move away from their initial position with their local velocity. This results in the ballistic t^2 regime. Next their vertical displacement is restricted to a thin layer. Particles perform wavelike motion that is also indirectly visible from the continuous increase and decrease of the vertical mean-squared displacement around an averaged plateau level [see Fig. 8(b)]. During this stage, particles continuously convert vertical kinetic energy into potential energy and vice versa.[16] In case the particles are released in a thin horizontal plane instead of as a homogeneous random distribution over the total domain, particle dispersion denotes the growth of the layer thickness. It is found in a separate simulation that particles released in this way will remain in a thin horizontal layer. For long times finally, due to the exchange of density between elements in the fluid by molecular processes, the actual equilibrium height of each individual particle slowly starts to deviate from its initial equilibrium height. Particles thus forget their initial positions, they obtain new equilibrium levels, and the resulting behavior is diffusive in the long-time limit.

The origin of the diffusive regimes found for dispersion in isotropic turbulence and in stratified turbulence is fundamentally different. In isotropic turbulence, the motion of a particle is purely advective. The linear dispersion behavior for long times is therefore a random-walk-like statistical property.[24] On the other hand, the diffusive regime for vertical single-particle dispersion in the case of strong stratification is caused by molecular diffusion of the density of the individual fluid particles. Without molecular diffusion, no long-time diffusion limit would be present.

The tool of tracking fluid elements can be used to study flow properties. As shown by Ref. 31, both particle trajectories (Lagrangian) and the diapycnal flux (Eulerian) can be used to derive the eddy diffusivity coefficient when studying mixing of a stably stratified flow. The diffusive regime for vertical dispersion in strongly stratified turbulence found in the present work gives a signature of irreversible mixing due to the diapycnal flux.

The quantitative differences in the long-time behavior of vertical dispersion between 2D and 3D forcing (Fig. 2) can be explained by differences in the flow dynamics. When forcing purely horizontally, mainly the vertical length scale is smaller than in the 3D-forced case. By rescaling the time axis with a large-scale advective time scale based on L_v and w' instead of scaling with $2\pi/N$, the long-time behavior becomes quite similar for both cases.

Horizontal dispersion is enhanced by stratification, as can be seen in Fig. 8(a). For long times, a clear superdiffusive regime is found that is proportional to t^α, with $\alpha=2.1\pm0.1$. The main cause of the presence of a superdiffusive regime is the effect of vertical shear. Stably stratified turbulence shows quasi-two-dimensional behavior. In the horizontal plane, large-scale vortical structures exist with large eddy turnover time scales. These horizontal structures are not fully decoupled in the vertical direction and strong shearing occurs between vortices in different layers. The vertical range of displacement of fluid particles is limited; in case N100, for example, a fluid particle traverses about 1/20 of the domain height. Locally the flow resembles a shear flow (see Fig. 4), and this shear causes superdiffusive dispersion behavior. Horizontal dispersion in flows with a constant mean vertical velocity gradient (linear shear), for example, is proportional t^3.[32] In the present study, we do not have pure shear flow only. Tests in which random-walk motion is carried out in profiles that resemble parts of the real vertical mean shear profile found in stratified turbulence (see Fig. 4) show the following. In a region of uniform flow [classical picture of a random walk, Fig. 10(a)], the long-time dispersion behaves like t; in linear shear flow [Fig. 10(b)], this gives t^3; and in the profile depicted in Fig. 10(c), the long-time dispersion limit scales proportional to t^2. It is therefore anticipated that the horizontal mean-square displacement in homogeneous stratified turbulence should scale like t^α, with $1<\alpha<3$.

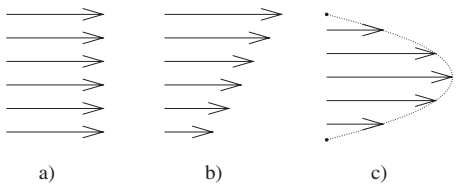

FIG. 10. Different simplified profiles that resemble parts of the mean vertical shear profile found for stratified turbulence (see Fig. 4). (a) Uniform flow, (b) linear shear flow, (c) one-half of a sine.

The influence of the Schmidt number on horizontal dispersion is negligible, which was expected because of the relative unimportance of density diffusion compared to advection.

B. Particle-pair dispersion

In view of future applications, in which aggregate formation (relevant for dispersion of micro-organisms) plays a role, not only single-particle statistics but also particle-pair statistics are of importance. For homogeneous isotropic turbulence, a couple of regimes can be identified for relative dispersion.[18,19] For short times, the mean-squared separation between two fluid elements grows either exponentially or like t^2. When the interparticle separation distance falls in the inertial range, this growth behaves as t^3 according to Richardson.[33] For long times, a diffusion limit exists similar to single-particle dispersion. Which regimes are passed through depends on the initial separation of the particles, only the final t regime is universal since at long times particles become uncorrelated, independent of their initial separation Δ_0. The t^3 regime is derived theoretically for high Reynolds number flows with a clear inertial range.[34]

The separation behavior for homogeneous isotropic turbulence (case N0) can be seen in Fig. 11 for an initial separation of about $\frac{3}{2}\eta$. A t^2 regime is expected initially and is indeed visible. Next follows a region that is close to t^3, though because of our relatively low Reynolds number this is a necessary transition from the t^2 regime to the t regime of

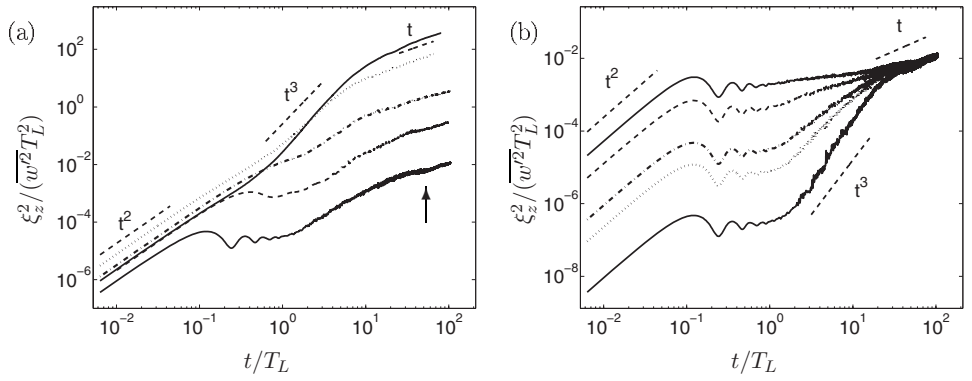

FIG. 11. Second-order moment of the vertical separation between two particles as a function of time. (a) Results for different levels of the background stratification, cases N0 (—), N1 (···), N10 (– · – · –), N100 (----), N1000 (—). The initial separations are in horizontal direction, $\frac{3}{2}\eta$ for cases N0 and N1000 and $\frac{5}{2}\eta$ for cases N1, N10, and N100. The first plateau starts around $t=2\pi/N$, whereas this value for the second plateau (indicated with an arrow) is $t\sim\mathcal{O}(T_E)=L_h/u_{\rm rms}$. In (b), case N1000 is shown for five different initial separations; $\frac{1}{6}\eta$ (—), $\frac{3}{4}\eta$ (···), $\frac{3}{2}\eta$ (– · – · –), 6η (----), 15η (—).

which the levels are determined by the flow instead of real Richardson dispersion. Moreover, this intermediate range with scaling close to t^3 is contaminated by the dissipative range because not all particles start separating at the same time. The pair dispersion is therefore a mixture of ballistic t^2 and t^3 behavior. This effect is demonstrated by Boffetta and Sokolov[35] and Biferale *et al.*,[36] who made use of the method of doubling times as introduced by Artale *et al.*[37] Finally, the long-term diffusion limit is clearly visible.

Figures 11 and 12 show pair dispersion in vertical ($\xi_z^2=\overline{[Z^{(1)}(t)-Z^{(2)}(t)]^2}$) and horizontal ($\xi_h^2=\frac{1}{2}\{\overline{[X^{(1)}(t)-X^{(2)}(t)]^2}+\overline{[Y^{(1)}(t)-Y^{(2)}(t)]^2}\}$) directions as a function of time, where superscripts 1 and 2 denote the two particles of a pair. These results are derived from pairs with an initial separation in directions perpendicular to the plotted dispersion direction, for example an initial separation in the horizontal plane for ξ_z^2. Results of pairs initially separated along the plotted direction are very similar, except for vertical cases in which Δ_0 in the z direction is larger than the levels of the first plateaus. Figure 11(a) shows that also in a stratified environment vertical separation starts with the classical t^2 regime. Next a plateau is found, starting around $t=2\pi/N$. At later times, an increase to a second plateau (indicated with an arrow) can be seen, at least for the strongest stratifications. The time at which the increase to this second plateau starts is of the order of the largest time scales in the flow (T_E). The final regime is again the linear diffusion limit. Nicolleau and Vassilicos[2] already predicted the existence of the second plateau, although their kinematic simulation was not carried out long enough to see more than just the beginning of this plateau. The transition from the first to the second plateau coincides with the intermediate t^3 regime for horizontal pair dispersion, when particles start moving apart in the horizontal. Although separation in vertical direction is limited, particles can freely disperse in horizontal direction. After some time, the horizontal separation is large enough for the two particles to become uncorrelated. The second plateau can therefore be associated with the plateau found for single-particle dispersion; the level of the second plateau is twice the level of the plateau for the dispersion of a single particle. The influence of initial separation is shown in Fig. 11(b). In general, the behavior is the same for different Δ_0. Especially for long times, its influence is rather small; a linear, uncorrelated behavior is seen at almost the same level. For very large initial separations in the horizontal plane, it is expected to see only one plateau, namely the second one. Already initially particles would reside in different structures within the flow, so there is no argument left for the existence of the first plateau. Indeed, our largest initial separation (15η) is much smaller than the horizontal extent of the dominant flow structures (L_h), and the first plateau is still present.

For horizontal pair dispersion, the effect of stratification

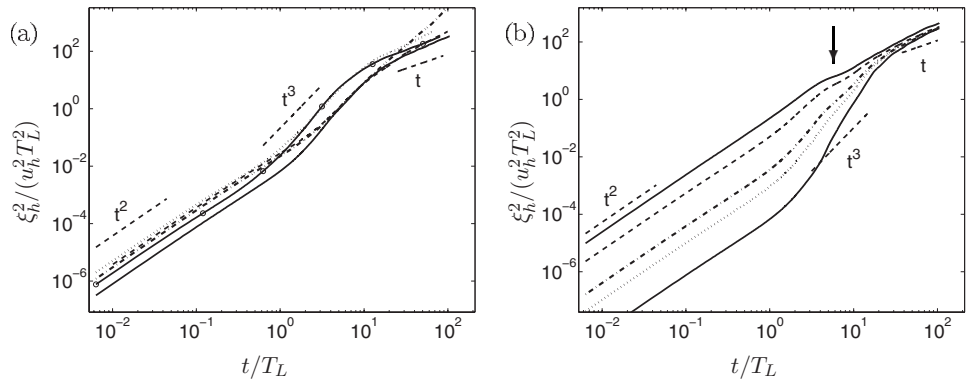

FIG. 12. Second-order moment of the horizontal separation between two particles as a function of time. (a) Results for different levels of the background stratification. The initial separations are $\frac{3}{2}\eta$ for cases N0 and N1000 and $\frac{5}{2}\eta$ for cases N1, N10, and N100. In (b), case N1000 is shown for five different initial separations. Lines as in Fig. 11, with –○– for case N0. The arrow points to anomalous behavior in the intermediate range for larger initial separations.

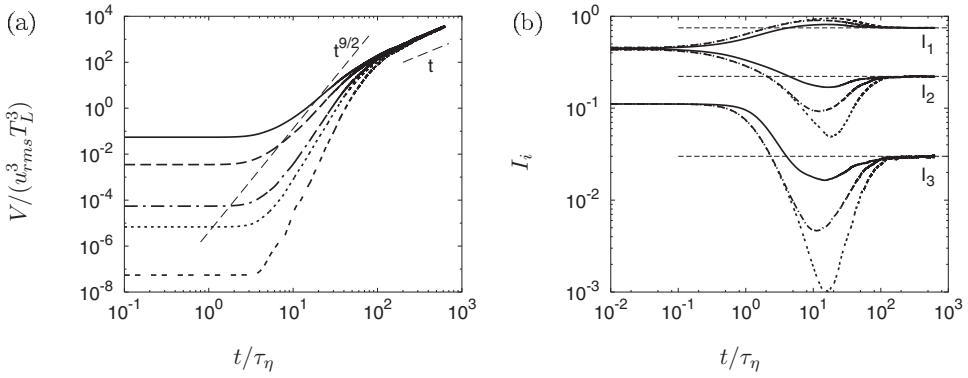

FIG. 13. (a) Volume as a function of time for different initial particle separations ($\frac{1}{6}\eta$: -- -- --, $\frac{3}{4}\eta$: ⋯, $\frac{3}{2}\eta$: – · – · –, 6η: ----, 15η: —). Richardson scaling would give $V \propto \epsilon^{3/2} t^{9/2}$ in the inertial range. (b) Eigenvalues I_1 (uppermost) to I_3 (lowest) as a function of time. For clarity, only three different initial cloud sizes are shown: $\frac{1}{6}\eta$, $\frac{3}{2}\eta$, and 15η, same lines as in (a). The horizontal lines give the Gaussian values $\langle I_1 \rangle_{G4} \approx 0.748$, $\langle I_2 \rangle_{G4} \approx 0.222$, and $\langle I_3 \rangle_{G4} \approx 0.03$. Both plots for case N0.

is less pronounced than for vertical pair dispersion, although the behavior is clearly altered compared to that in isotropic turbulence. As can be seen in Fig. 12(a), the start of the intermediate range is shifted toward larger times and the long-term behavior of case N10 in particular differs from the isotropic case. For long times, the particles forming a pair become uncorrelated. This would lead to the same dispersion behavior as for single particles, which is superdiffusive. Contrary to single-particle dispersion, here the graphs tend toward a linear slope or slightly steeper for long times, except for case N10, where the slope remains $\mathcal{O}(t^{2.5})$. Longer integration times are needed to draw a final conclusion about the long-term behavior of horizontal particle-pair dispersion. The onset of the long-time dispersion behavior shifts toward larger times for pair dispersion compared to single-particle dispersion, as can be illustrated by the shift in time between the related plateaus for vertical single-particle dispersion and vertical particle-pair dispersion. The long-time horizontal particle-pair dispersion with possible superdiffusive behavior is not captured in the present simulations.

When looking at the influence of initial separation (Fig. 12(b)), it can be seen that also in the intermediate range stratification influences horizontal pair dispersion, at least for case N1000. For the largest initial separations, a small bump is found in the intermediate range, around $t/T_L=5$. This time coincides with the time at which the strongly stratified cases start to deviate from the isotropic case for single-particle dispersion in horizontal direction.

C. Multiparticle statistics

The evolution of a cluster of four particles is studied to get an idea of the shape dynamics of clouds of particles in stably stratified turbulence. Under the action of the flow field, the cloud deforms, and in this way the shape of the cloud can also be used to characterize the flow field. The analysis of multiparticle statistics in this work is conducted along the same lines as in previous work on homogeneous isotropic turbulence.[21,22] In order to characterize the shape dynamics for a set of $M=4$ particles, the following set of vectors is introduced:[38]

$$\boldsymbol{r}_0 = (\boldsymbol{x}_{p,1} + \boldsymbol{x}_{p,2} + \boldsymbol{x}_{p,3} + \boldsymbol{x}_{p,4})/2, \tag{17}$$

$$\boldsymbol{r}_1 = (\boldsymbol{x}_{p,2} - \boldsymbol{x}_{p,1})/\sqrt{2}, \tag{18}$$

$$\boldsymbol{r}_2 = (2\boldsymbol{x}_{p,3} - \boldsymbol{x}_{p,2} - \boldsymbol{x}_{p,1})/\sqrt{6}, \tag{19}$$

$$\boldsymbol{r}_3 = (3\boldsymbol{x}_{p,4} - \boldsymbol{x}_{p,3} - \boldsymbol{x}_{p,2} - \boldsymbol{x}_{p,1})/\sqrt{12} \tag{20}$$

with $\boldsymbol{x}_{p,i}$ $(i=1,M)$ the particle positions at the vertices of initially regular (but not isotropic) tetrahedra. $\boldsymbol{r}_0$ defines the center of mass of the cluster, which has no influence on the cluster shape because of homogeneity of the flow and the uniform initial particle distribution. Vectors $\boldsymbol{r}_1$ to $\boldsymbol{r}_3$ form the columns of a square matrix $\boldsymbol{r}$ from which a moment of inertialike tensor $\boldsymbol{I}=\boldsymbol{r}\boldsymbol{r}^T$ can be defined. The radius of gyration $R^2=\Sigma_{i=1}^{M-1}\boldsymbol{r}_i^2=\mathrm{tr}\boldsymbol{I}=g_1+g_2+g_3$ measures the spatial extent of the swarm of particles. The shape of the cluster of particles can be derived from the eigenvalues g_i $(g_1 \geqslant g_2 \geqslant g_3)$ of matrix $\boldsymbol{I}$. Often these eigenvalues are given as the ratio $I_i=g_i/R^2$ (obviously $I_1+I_2+I_3=1$). For the case $M=4$, $g_1=g_2=g_3$ corresponds to an isotropic object. When $g_1 \approx g_2 \gg g_3$, the object is flattened in one direction and has a pancake-like shape and $g_1 \gg g_2, g_3$ represents a needlelike object. Convenient ways to describe the overall shape of an object consist of monitoring I_2 or the volume $V=\|\det(\boldsymbol{r})\|$ of the object.[21] Using Monte Carlo simulations, Pumir *et al.*[21] and Biferale *et al.*[22] derived the values $\langle I_2 \rangle_{G4} \approx 0.222$ and $\langle I_3 \rangle_{G4} \approx 0.03$ for an isotropic Gaussian particle distribution, from which it follows that $\langle I_1 \rangle_{G4} \approx 0.748$. Instead of looking only at mean values, a good description of the type of structures occurring in a certain flow is also given by the probability density function (pdf) of the eigenvalues I_i.

The procedure described above is first applied to case N0, homogeneous isotropic turbulence. The results from that case can be compared to previous work by Pumir *et al.*[21] and Biferale *et al.*[22] and they serve as a reference when studying the shape evolution of particle clouds in stratified turbulence. The results correspond nicely with Fig. 1 in Pumir *et al.*[21] and Fig. 2 in Biferale *et al.*[22] In Fig. 13, the volume V and scaled eigenvalues I_i are shown as a function of time for different initial cloud sizes. Time is scaled by the Kolmogorov time τ_η for comparison with literature.[21,22] The ratio of τ_η/T_L is $\mathcal{O}(10^{-1})$. For each different case shown in the figure, the results are ensemble averages over 4096 tetrads. The volume of the tetrahedra grows in time, where the start of the growth occurs slightly earlier for larger Δ_0. In the intermediate range, no convincing $t^{9/2}$ regime (Richardson) is found. This is due to the same reasons as mentioned for particle-pair

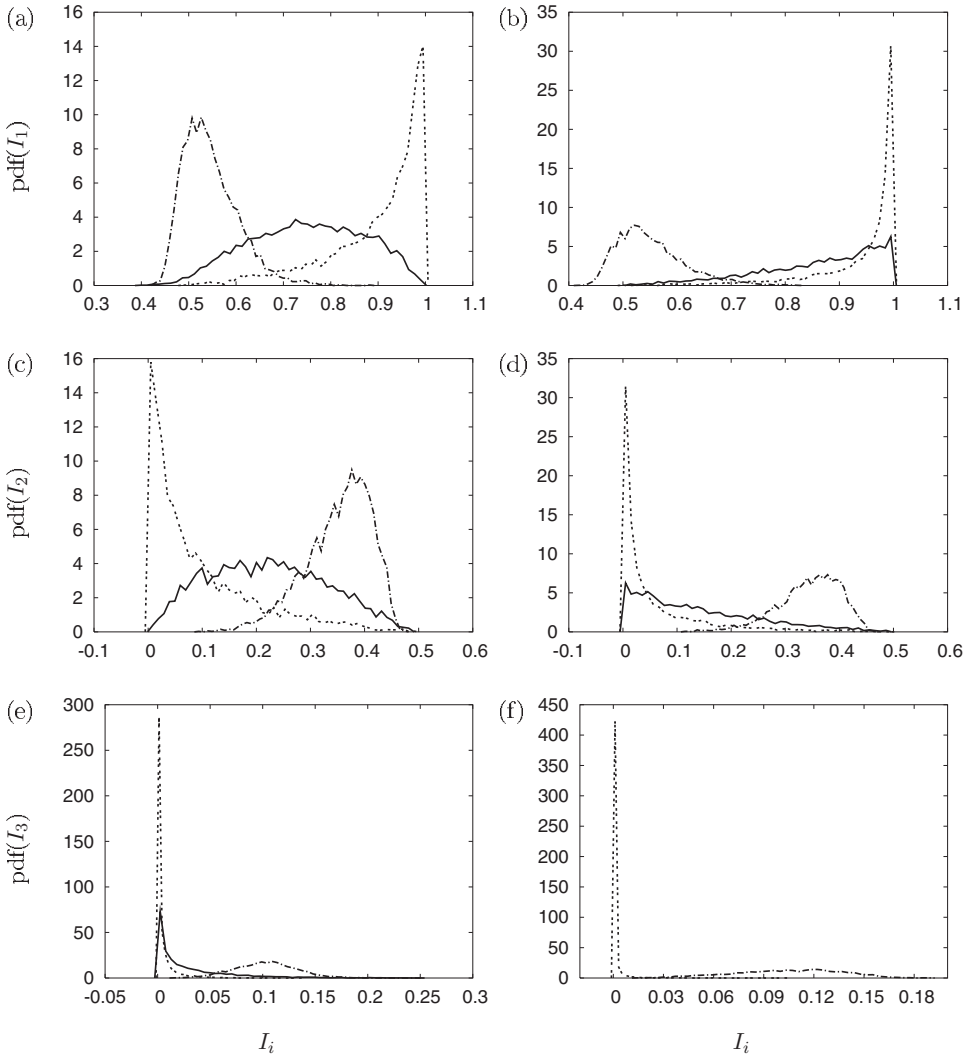

FIG. 14. Probability density function of the eigenvalues I_i at three different times: $t/\tau_\eta = \mathcal{O}(0.5)$: – · – · –, $t/\tau_\eta = \mathcal{O}(15)$: -- -- --, $t/\tau_\eta = \mathcal{O}(500)$: —. Left column shows results for case N0 $(\Delta_0 = \frac{3}{2}\eta)$, right column for case N100 $(\Delta_0 = \frac{5}{2}\eta)$. For case N100, the final pdf for I_3 is left out, because it is only a sharp peak around zero.

separation statistics (see Sec. IV B). For long times, diffusive growth can be seen, related with the uncorrelated motion of the particles that form a tetrahedron. Our results cover a much larger time range than those of Pumir *et al.*[21] and Biferale *et al.*,[22] making it possible to find this long-time diffusive behavior, not only for the volume but also for the unscaled eigenvalues g_i (not shown). Looking at the eigenvalues, it can be seen that initially I_2 and I_3 decrease and I_1 increases. The maximum distortion is reached around $t/\tau_\eta = \mathcal{O}(10)$; the ratio of the eigenvalues $I_1:I_2:I_3$ is then approximately $10^0:10^{-1}:10^{-2}$ (exact values depend on initial separation). This moment falls in the intermediate range, when the growth of the volume is strongest. Geometrically it means that the tetrahedra change from their initial regular shape to more pancake-like and even needlelike structures. They are strongly elongated. For long times, they relax nicely toward the Gaussian values mentioned earlier. Different initial particle separations, or equivalently different initial tetrahedron sizes, result in differences in both the moment of maximum distortion and in its value. With decreasing Δ_0, distortion increases, denoting more deformation. Because the smallest tetrahedra need more time for their size to reach the scales of the intermediate range (volume starts growing later), it is expected that smaller tetrahedra reach the peak eigenvalues at later times than larger ones. For the smallest three Δ_0 this is indeed found, however for larger Δ_0 $(6\eta, 15\eta)$ the instants of time of maximum distortion increase again. Of course, at a single moment in time all kinds of shapes are possible. The graph shown so far only gives an idea of the mean shape of the objects in the flow. Plots of the probability density function give a good picture of the types of structures occurring at different times during the evolution. For an initial cloud size of the order of the Kolmogorov size, the pdfs of I_1 to I_3 are plotted on the left-hand side of Fig. 14. This is done for three different times: one shortly after the release of the particles in the flow, one around the moment of maximum distortion, and one for the long-time limit. A strong change with time can be seen. The shift of the peak toward larger (I_1) and smaller (I_2, I_3) values already became clear from plots of the averaged values (Fig. 13). The sharpest distributions are found around $t/\tau_\eta = \mathcal{O}(10)$, where the peaks occur in the graphs of I_i. For long times, a considerable amount of tetrahedra has values for I_1 of the order of 0.5–0.6, and values for I_2 of about 0.4–0.5. This means that a reasonable amount of the tetrads (about 10%)

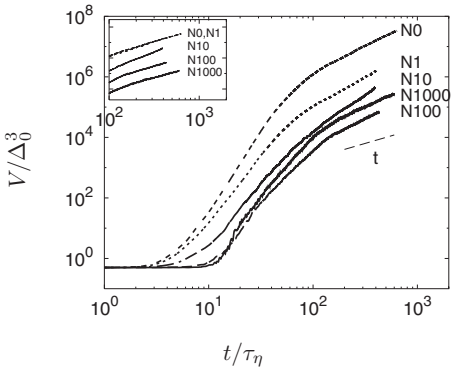

FIG. 15. Volume as a function of time for different strengths of the stratification: (N0: -- -- --, N1: ⋯, N10: – · – · –, N100: ----, N1000: —). Volume is scaled by the initial particle separation Δ_0. The choice of this scaling leads to the fact that the graph of case N1000 lies above that of case N100 for long times ($\Delta_{0,N1000} < \Delta_{0,N100}$). The inset shows the long-time behavior when scaled with $u_{\mathrm{rms}}^3 T_L^3$; now cases N0 and N1 collapse and the order is as expected.

have a shape that is more two-dimensional than the average value of the eigenvalues would predict. I_3 is strongly peaked around zero, so few real three-dimensional structures exist.

Stable stratification suppresses vertical motion in the flow, resulting in less particle dispersion in vertical direction. When tetrahedra are placed in such a flow, it is expected that their shapes will become quasi-two-dimensional. The effect of stratification on the volume growth of a cluster of four particles can be seen in Fig. 15. With increasing stratification strength, the time at which tetrads start growing increases. Furthermore, it follows that with increasing stratification, the volume of a cloud decreases. Case N1000 seems to be an exception to this finding, but that is due to the chosen scaling with Δ_0, which is well-suited for short times. When scaled with large-scale properties such as T_L and u_{rms}, the order of the graphs for long times is as expected; the lowest graph then belongs to case N1000. Cases N1, N10, and N100 do not (yet) reach a final linear regime. For the strongest stratification studied in this work, the influence of initial cloud size on the growth of the cloud is shown in Fig. 16(a). As opposed to the isotropic case N0, for long times a difference can still be found here between different initial particle separations. The smallest three Δ_0 reach similar cloud sizes, although their growth there is not equally strong. The smallest Δ_0 does not (yet) show a final diffusive regime. The nondiffusiveness is presumably associated with the nondiffusive long-time horizontal single-particle dispersion.

TABLE III. Asymptotic eigenvalues for different levels of the stratification. Values for I_3 are left out for cases N10, N100, and N1000; they are approximately zero.

Case	I_1	I_2	I_3
N0	0.747 ± 0.002	0.222 ± 0.002	0.029 ± 0.001
N1	0.808 ± 0.006	0.179 ± 0.004	0.014 ± 0.004
N10	0.89 ± 0.03	0.11 ± 0.03	
N100	0.856 ± 0.004	0.143 ± 0.004	
N1000	0.841 ± 0.003	0.158 ± 0.004	

The vertical direction, which is suppressed by stratification, plays a considerable role in the growth of a cloud. Even though in isotropic turbulence structures become mainly two-dimensional, the smaller volumes for stronger stratification point to even flatter structures in stably stratified turbulence. This is indeed the case, as can be concluded from the eigenvalues. For case N1000 in Fig. 16(b), the scaled eigenvalues I_i are given as a function of time for different initial particle separations. It can be seen that $I_3 \approx 0$, $I_1 > \langle I_1 \rangle_{G4}$, and $I_2 < \langle I_2 \rangle_{G4}$. So the structures are more flattened than in the isotropic case. The time it takes to reach a final distribution is much longer than for case N0, and this distribution remains a bit unsteady. The influence of initial separation is similar to the case of isotropic turbulence. More generally, it can be concluded that with increasing N, I_1 increases, I_2 decreases, and I_3 converges to zero, resulting in flatter and more elongated structures. The long-time asymptotic values of the three eigenvalues are given in Table III for the different stratification levels. For all stratified cases, the long-time behavior of the eigenvalues is less stable than for case N0. Case N10, however, does not reach steady state within the duration of the simulation. The values given in the table for case N10 are therefore only rough estimates. The slight increase of I_1 and decrease of I_2 for case N1000 compared to case N100 can be caused by different initial particle separations ($\frac{3}{2}\eta$ and $\frac{5}{2}\eta$, respectively). The values for I_1 and I_2 can also be compared with the Gaussian values derived for multiparticle statistics in two-dimensional turbulent flow. Since the asymptotic value of I_3 is approximately zero for the strongly stratified cases, an option would be to compare the first two eigenvalues with the two eigenvalues that result from three-

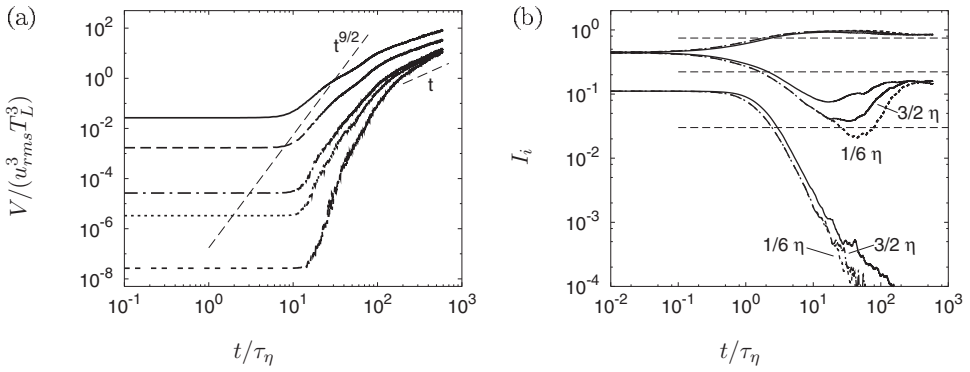

FIG. 16. For strongly stratified turbulence (case N1000), the volume (a) and eigenvalues I_i (b) are shown as a function of time for different initial particle separations. Lines as in Fig. 13. These plots look a bit wobbly because of the limited amount of tetrahedron used to calculate statistics.

particle statistics in two-dimensional turbulence. This topic was studied by Castiglione and Pumir,[39] who derived $\langle I_2\rangle_{G3,2D}\approx 0.107$ and thus $\langle I_1\rangle_{G3,2D}\approx 0.893$. The values found for four-particle statistics in stably stratified turbulence then lay in between those for four-particle statistics in isotropic 3D turbulence and three-particle statistics in 2D turbulence. Furthermore, we looked at three-particle statistics for case N100. Independent of the initial particle configuration, a purely horizontal or purely vertical triangle, the asymptotic value for I_2 is now 0.097. Comparing this value with the above-mentioned value for 2D turbulence ($\langle I_2\rangle_{G3,2D}\approx 0.107$) and with the Gaussian result for three-particle statistics in 3D isotropic turbulence, $\langle I_2\rangle_{G3,3D}=1/6$,[21] our result resembles that for 2D turbulence.

For case N100, probability density functions of the eigenvalues I_i are derived, and shown on the right-hand side of Fig. 14. All three eigenvalues show a peak around the time of maximum distortion that is much sharper than for case N0. Also for long times there is less spreading in the values of I_i. The distribution of eigenvalue I_1 is shifted toward 1 and that of eigenvalue I_2 towards zero. Eigenvalue I_3 only shows a very sharp peak close to zero. These values are a confirmation of the picture of flatter and more prolonged tetrahedra compared to isotropic turbulence. Moreover, it shows that the spectrum of structures occurring in stratified turbulence is less broad. For example, tetrads with $I_1\approx I_2$, denoting flat but not elongated shapes, are hardly found.

V. CONCLUDING REMARKS

Forced direct numerical simulations provide a means to study fluid particle dispersion in statistically stationary stably stratified turbulence. Stratification suppresses vertical fluid motion in turbulent flows. With increasing strength of the stratification, less and less small-scale motion and overturning is present in the flow. Suppression of vertical motion leads to the occurrence of plateaus in plots of both vertical single-particle and particle-pair dispersion. For long times, however, an increase in vertical dispersion is found approaching the linear diffusion limit as seen in isotropic turbulence. This regime is caused by molecular diffusion of the active scalar, the density ρ, which slowly changes the equilibrium height of the particles. In horizontal direction, dispersion is enhanced for long times, especially for single-particle dispersion.

When looking at clusters of four particles, representing particle clouds, the method of deriving eigenvalues of the moment of inertialike tensor works well to describe shape evolution. Compared to isotropic turbulence, in stably stratified turbulence deformation of tetrahedra is enhanced. Structures tend to become more flattened and elongated and their volume decreases with increasing stratification. Moreover, the spreading in types of structures is much smaller than in isotropic turbulence.

The dispersion results presented in this work can be important for practical purposes. Both the suppression of vertical dispersion and the inhibition of cloud growth might enhance clustering and aggregation for interacting particles, because particles remain close together for longer times. On the other hand, the final diffusion limit found here makes it possible for particles to reach everywhere in the flow for long enough times.

To study dispersion in realistic geophysical environments, instead of passive fluid particles, particles with physical properties need to be studied. As a next step, we will include mass and inertial effects to study their influence on particle dispersion. Furthermore, the investigation of collisions and aggregate formation in stratified turbulence is left for future work.

ACKNOWLEDGMENTS

This programme is funded by the Netherlands Organisation for Scientific Research (NWO) and Technology Foundation (STW) under the Innovational Research Incentives Scheme Grant No. ESF.6239. This work was sponsored by the Stichting Nationale Computerfaciliteiten (National Computing Facilities Foundation, NCF) for the use of supercomputer facilities, with financial support from the Nederlandse Organisatie voor Wetenschappelijk Onderzoek (Netherlands Organisation for Scientific Research, NWO).

[1] Y. Kimura and J. R. Herring, "Diffusion in stably stratified turbulence," J. Fluid Mech. **328**, 253 (1996).
[2] F. Nicolleau and J. C. Vassilicos, "Turbulent diffusion in stably stratified non-decaying turbulence," J. Fluid Mech. **410**, 123 (2000).
[3] L. Liechtenstein, F. S. Godeferd, and C. Cambon, "Nonlinear formation of structures in rotating stratified turbulence," J. Turbul. **6**, 1 (2005).
[4] L. Liechtenstein, F. S. Godeferd, and C. Cambon, "The role of nonlinearity in turbulent diffusion models for stably stratified and rotating turbulence," Int. J. Heat Fluid Flow **27**, 644 (2006).
[5] H. J. Pearson, J. S. Puttock, and J. C. R. Hunt, "A statistical model of fluid-element motions and vertical diffusion in a homogeneous stratified turbulent flow," J. Fluid Mech. **129**, 219 (1983).
[6] J. J. Riley and M.-P. Lelong, "Fluid motions in the presence of strong stable stratification," Annu. Rev. Fluid Mech. **32**, 613 (2000).
[7] J. R. Herring and O. Métais, "Numerical experiments in forced stably stratified turbulence," J. Fluid Mech. **202**, 97 (1989).
[8] M. L. Waite and P. Bartello, "Stratified turbulence dominated by vortical motion," J. Fluid Mech. **517**, 281 (2004).
[9] E. Lindborg, "The energy cascade in a strongly stratified fluid," J. Fluid Mech. **550**, 207 (2006).
[10] P. K. Yeung, "Lagrangian investigations of turbulence," Annu. Rev. Fluid Mech. **34**, 115 (2002).
[11] P. K. Yeung and S. B. Pope, "Lagrangian statistics from direct numerical simulations of isotropic turbulence," J. Fluid Mech. **207**, 531 (1989).
[12] L. Biferale, G. Boffetta, A. Celani, A. Lanotte, and F. Toschi, "Particle trapping in three-dimensional fully developed turbulence," Phys. Fluids **17**, 021701 (2005).
[13] I. M. Mazzitelli and D. Lohse, "Lagrangian statistics for fluid particles and bubbles in turbulence," New J. Phys. **6**, 203(2004).
[14] M. Bourgoin, N. T. Ouellette, H. Xu, J. Berg, and E. Bodenschatz, "The role of pair dispersion in turbulent flow," Science **311**, 835 (2006).
[15] S. Ott and J. Mann, "An experimental investigation of the relative diffusion of particle pairs in three-dimensional turbulent flow," J. Fluid Mech. **422**, 207 (2000).
[16] S. K. Venayagamoorthy and D. D. Stretch, "Lagrangian mixing in decaying stably stratified turbulence," J. Fluid Mech. **564**, 197 (2006).
[17] G. T. Csanady, "Turbulent diffusion in a stratified fluid," J. Atmos. Sci. **21**, 439 (1964).
[18] B. Sawford, "Turbulent relative dispersion," Annu. Rev. Fluid Mech. **33**, 289 (2001).
[19] P. K. Yeung and M. S. Borgas, "Relative dispersion in isotropic turbulence. Part 1: Direct numerical simulations and Reynolds-number dependence," J. Fluid Mech. **503**, 93 (2004).
[20] B. Lüthi, A. Tsinober, and W. Kinzelbach, "Lagrangian measurement of vorticity dynamics in turbulent flow," J. Fluid Mech. **528**, 87 (2005).
[21] A. Pumir, B. I. Shraiman, and M. Chertkov, "Geometry of Lagrangian

dispersion in turbulence," Phys. Rev. Lett. **85**, 5324 (2000).
[22]L. Biferale, G. Boffetta, A. Celani, B. J. Devenish, A. Lanotte, and F. Toschi, "Multiparticle dispersion in fully developed turbulence," Phys. Fluids **17**, 111701 (2005).
[23]K. B. Winters, J. A. MacKinnon, and B. Mills, "A spectral model for process studies of rotating, density-stratified flows," J. Atmos. Ocean. Technol. **21**, 69 (2004).
[24]P. A. Davidson, *Turbulence: An Introduction for Scientists and Engineers* (Oxford University Press, Oxford, 2004).
[25]E. Lindborg and G. Brethouwer, "Stratified turbulence forced in rotational and divergent modes," J. Fluid Mech. **586**, 83 (2007).
[26]G. Brethouwer, P. Billant, E. Lindborg, and J.-M. Chomaz, "Scaling analysis and simulation of strongly stratified turbulent flows," J. Fluid Mech. **585**, 343 (2007).
[27]P. Billant and J.-M. Chomaz, "Self-similarity of strongly stratified inviscid flows," Phys. Fluids **13**, 1645 (2001).
[28]E. J. Strang and H. J. S. Fernando, "Entrainment and mixing in stratified shear flows," J. Fluid Mech. **428**, 349 (2001).
[29]S. B. Pope, *Turbulent Flows* (Cambridge University Press, Cambridge, UK, 2000).
[30]Y. Kaneda and T. Ishida, "Suppression of vertical diffusion in strongly stratified turbulence," J. Fluid Mech. **402**, 311 (2000).
[31]P. Bouruet-Aubertot, C. Koudella, C. Staquet, and K. B. Winters, "Particle dispersion and mixing induced by breaking internal gravity waves," Dyn. Atmos. Oceans **32**, 95 (2001).
[32]S. Corrsin, "Progress report on some turbulent diffusion research," Adv. Geophys. **6**, 161 (1959).
[33]L. F. Richardson, "Atmospheric diffusion shown on a distance-neighbour graph," Proc. R. Soc. London, Ser. A **110**, 709 (1926).
[34]A. S. Monin and A. M. Yaglom, *Statistical Fluid Dynamics*, *Vol.* 2 (MIT Press, Cambridge, MA, 1975).
[35]G. Boffetta and I. M. Sokolov, "Relative dispersion in fully developed turbulence: The Richardson's law and intermittency corrections," Phys. Rev. Lett. **88**, 094501 (2002).
[36]L. Biferale, G. Boffetta, A. Celani, B. J. Devenish, A. Lanotte, and F. Toschi, "Lagrangian statistics of particle pairs in homogeneous isotropic turbulence," Phys. Fluids **17**, 115101 (2005).
[37]V. Artale, G. Boffetta, A. Celani, M. Cencini, and A. Vulpiani, "Dispersion of passive tracers in closed basins: Beyond the diffusion coefficient," Phys. Fluids **9**, 3162 (1997).
[38]M. Chertkov, A. Pumir, and B. I. Shraiman, "Lagrangian tetrad dynamics and the phenomenology of turbulence," Phys. Fluids **11**, 2394 (1999).
[39]P. Castiglione and A. Pumir, "Evolution of triangles in a two-dimensional turbulent flow," Phys. Rev. E **64**, 056303 (2001).